Journal of Cellular Plastics

http://cel.sagepub.com

Process-structure Relationships in PCL Foaming

Carlo Marrazzo, Ernesto Di Maio, Salvatore Iannace and Luigi Nicolais

Journal of Cellular Plastics 2008; 44; 37
DOI: 10.1177/0021955X07079147

The online version of this article can be found at:
http://cel.sagepub.com/cgi/content/abstract/44/1/37

Published by:
SAGE
http://www.sagepublications.com

Process-structure Relationships in PCL Foaming

CARLO MARRAZZO,[1] ERNESTO DI MAIO,[1,*] SALVATORE IANNACE[2] AND LUIGI NICOLAIS[1,2]

[1]*Department of Materials and Production Engineering, Faculty of Engineering University of Naples Federico II, P.le Tecchio 80, 80125 Naples, Italy*

[2]*Institute of Composite and Biomedical Materials, National Research Council of Italy, P.le E. Fermi 1, 80055 Portici (Na), Italy*

ABSTRACT: The foaming behavior of poly(ε-caprolactone) (PCL) with nitrogen as the foaming agent has been investigated. By using a uniquely designed and instrumented batch foaming apparatus it is possible to study the correlation between the foam structure (i.e., foam density and mean cell diameter) and the main processing variables (i.e., foaming temperature, foaming agent concentration, and pressure drop rate). A narrow experimental range has been used to describe the complex dependencies by a simple model. In particular, linear algebraic functions have been used to describe the effect of the processing variables on both the foam density and the mean cell diameter. With the aim to better depict these relationships, 3D graphs are also reported. This visualization/parametrization allows the rapid selection of the proper process parameters to obtain PCL foams with the desired density and morphology.

KEY WORDS: PCL, nitrogen, foaming, process variables, model.

INTRODUCTION

Polymeric foams are two-phase materials in which a great number of gas-filled cells are entrapped in a macromolecular phase. These heterogeneous materials have a combination of properties that make them attractive for a wide range of applications in different industrial fields, in particular when good mechanical properties

*Author to whom correspondence should be addressed. E-mail: edimaio@unina.it
Figures 1, 4 and 5 appear in color online: http://cel.sagepub.com

0021-955X/08/01 0037–16 $10.00/0 DOI: 10.1177/0021955X07079147

Los Angeles, London, New Delhi and Singapore

and low weight need to be coupled. Typical examples are packaging, medicine, transport, acoustic, and thermal insulation and damping [1,2].

In the past two decades many authors have extensively studied the foaming behavior of a great number of polymers (e.g., polypropylene [3–7], polystyrene [8–11], and polycarbonate [12–14]) with environmentally benign gases, such as carbon dioxide or nitrogen, but few studies have been conducted on the production of foams with biodegradable polymeric matrices [15–21]. Detailed analyses of the foaming process, in terms of the effect of processing parameters on the final foam structure, have been conducted. The main process parameters are suggested by the classical nucleation theory [22] which provides the nucleation rate of bubbles in a polymer–gas solution as function of the gas molecules concentration (ω_{sat}), the temperature at which the thermodynamic instability promoting bubble nucleation is induced (T_{foam}) and the difference between the gas pressure prior to foaming and the final pressure (ΔP). In the following, the effects of the single main process parameters are briefly reviewed, by describing the process-final foam structure dependence.

The gas concentration in the polymeric solution prior to foaming has an important effect on the structure, both on the morphology (mainly referred to as the pore number per cubic centimeter of unfoamed material, also called the cell number density) and on the final foam density [12,13,23,24]. It has been observed, in particular, that an increase in the gas concentration led to an increase of the cell number density. Most of the authors, in particular, reported that this dependence decreases with the increase of the concentration and, eventually, reached a plateau, depending on the materials and on the investigated experimental ranges. A two order of magnitude increase of the cell number density was reported for extruded PS/CO_2 system [11] with the increase of the gas concentration from 2 to 10% wt. On extrusion foamed PP/CO_2 system [3], a five order of magnitude increase has been observed with an increase of ω_{sat} from 1 to 11%. Similar results were achieved on foams prepared via a batch process on PS/CO_2 by Arora et al. [9]. However, in their batch process, the effect of ω_{sat} in equilibrium at saturation pressure, P_{sat}, is coupled to the effect of the pressure drop rate ($\Delta \dot{P}$), that is the rate at which the pressure inside the vessel is released, which has a non-negligible effect on foaming as will be reported in the following. The gas concentration, as expected and extensively reported [9,12,13,23], has a great effect on the final foam density too, since the higher the gas availability to inflate bubbles, the lower the final density. The limit to this density reduction is the capability of the polymeric matrix to withstand the elongational

deformation during cell growth; if this limit is exceeded, cell collapse and foam densification occur.

Foaming temperature can be considered as the main processing parameter. In fact the processing temperature windows include foaming temperatures that are low enough to prevent cell coalescence and high enough to prevent premature crystallization/vetrification. In the foaming window, whatever the expanding polymer/gas system, foam density has the classical bell shape, with high-density values in the extremes [6,12,13,24,25]; conversely, most of the authors reported a little or negligible effect of temperature on the cell nucleation density [11,23,26].

As mentioned earlier, a further process parameter which is not directly accounted for in the classical nucleation theories but, in practice, extensively affects foam morphology, is the pressure drop rate. One to two orders of magnitude increase in cell number density with the increase of $\Delta\dot{P}$ by two or three orders of magnitude has been observed in several polymer/gas systems [9,11,13,14], while the effect on the final foam density is often negligible, as it could be expected.

Despite the wide literature on the subject, however the relationships between process and structure in thermoplastic foaming seem not to be clear. Furthermore, single results are not applicable or, at least, transferred to different polymer/blowing agent system, in particular with regard to the coupling effects of the processing variables.

In this study, the foaming behavior of poly(ε-caprolactone) (PCL)/N_2 system was investigated. The influence of the aforementioned three main process parameters – gas mass fraction, foaming temperature, and pressure drop rate – on the density and the cellular structure of the final foam was analyzed. To this aim a batch foaming apparatus was designed in order to independently control the three process variables and define a foaming protocol. In particular, saturation pressure and pressure drop rate were decoupled by using a controlled gas release system. As a consequence, PCL foams with a controlled density and morphology were obtained.

EXPERIMENTALS

Materials

The polymer/gas system under investigation is constituted by PCL as the biodegradable matrix and N_2 as the foaming agent.

Poly(ε-caprolactone) is an aliphatic thermoplastic polyester, biodegradable in several biotic environments. Its nontoxicity versus biological

tissues [27] makes it interesting in drug delivery systems [18] and tissue engineering [28]. Moreover, it has potential application in food packaging and agriculture [29]. The PCL used in this work is CAPA 6800 (Solvay Interox Ltd., Southampton, UK), used as received. The molecular weight and melt flow index, as reported by Solvay, are 80000 and 3 g/10 min (at temperature 160°C and pressing mass of 2.16 kg), respectively. The room conditions density is equal to 1.14 g/cm^3. T_g is −60°C and T_m is 60°C. The crystallization temperature (as measured by DSC at −10°C/min) is around 30°C. Commercial purity grade N_2 (Sol, Italy) was used as foaming agent.

Batch Foaming Apparatus

For the preparation of foam samples, a thermo regulated and pressurized cylinder having a volume of 0.3 L, (HiP, model BC-1) was used. It was suitably modified to allow a careful measurement and control of the three process parameters of interest. Figure 1 reports a photograph and a scheme of the batch foaming apparatus used in this study. For the temperature control, an electrical heater (no. 11, in Figure 1) as heating element, and a heat exchanger with an oil bath (no. 12) as cooling element, were used. They were controlled by a PID thermoregulator (Ascon, model X1), which reads the temperature inside the vessel by using a Pt100 (no. 4). A pressure transducer (Schaevitz, model P943) (no. 3) was used to measure pressures during saturation step and to register pressure histories during blowing agent discharge. The pressure discharge system consists of a discharge valve (HiP ball valve, model 15-71 NFB), an electromechanical actuator (HiP, model 15-72 NFB TSR8) (no. 6), and an electrovalve (no. 7–9). This system allowed reproducibility in valve opening. The discharge valve was connected to capillaries of different length and/or diameter (a set of nine capillaries was used), (no. 5) in order to change pressure drop rates independently from the saturation pressure. The pressure history, $P(t)$, was registered by using a data acquisition system (DAQ PCI6036E, National Instruments, Austin, TX, USA) and, finally, pressure drop rate was calculated as the highest absolute value of the derivative of $P(t)$.

Foam Preparation

Typical experiments were conducted using the following procedure: PCL samples 5 mm thick, with a diameter of 15 mm were saturated at 75°C with the foaming agent at saturation pressure P_{sat}, for 6 h.

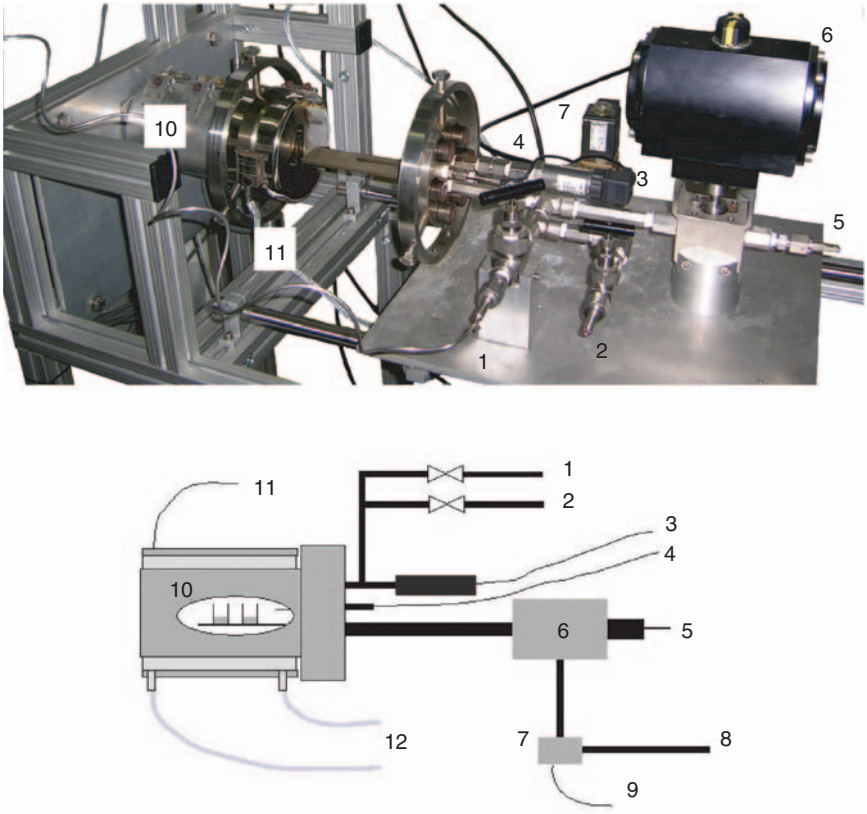

Figure 1. Photograph and scheme of the batch foaming apparatus; (1) to gas cylinder; (2) to vacuum pump; (3) pressure transducer output, to data acquisition system; (4) Pt100 for temperature measurement and control, to data acquisition system and PID controller; (5) exchangeable capillary; (6) actuated ball valve; (7) electrovalve; (8) pressure inlet to actuate the ball valve; (9) electrovalve control; (10) section of the vessel (sample holders and Pt100 sensor positioning); (11) electric heater input, PID controlled; (12) to oil bath, PID controlled.

The vessel was then cooled to the foaming temperature, T_{foam}, with a controlled, repeatable cooling history, and finally pressure-quenched to ambient pressure, using different pressure drop rates, $\Delta\dot{P}$. All of the experiments were conducted at the same saturation temperature and, therefore, at the end of gas-saturation step, gas mass fraction in the polymeric matrix, ω_{sat}, and saturation pressure, P_{sat}, are univocally correlated and can be used indifferently as a unique processing variable. In the following, we refer to P_{sat}.

Table 1. Complete set of experiments.

Test	P_{sat} (bar)	$\Delta\dot{P}$(bar/s)	T_{foam} (°C)
A	140	260	44.5
B	140	320	46.5
C	140	380	48.5
D	170	380	44.5
E	170	260	46.5
F	170	320	48.5
G	200	320	44.5
H	200	380	46.5
I	200	260	48.5
L	140	260	48.5

Table 2. Measured and predicted densities and cell sizes.

Test	Measured density (kg/m^3)	Predicted density (kg/m^3)	Measured cell size (μm)	Predicted cell size (μm)
A	213	204	161	163
B	200	198	142	171
C	194	191	387	179
D	194	203	40	79
E	178	197	87	123
F	200	190	90	131
G	231	202	53	31
H	179	196	56	39
I	200	190	87	83
L	204	191	239	203

A convenient set of experiments was used to correlate the foaming behavior of the system to the main process parameters (Table 1). Three values for each of the processing variables have been used: P_{sat} (140, 170, and 200 bar), T_{foam} (44.5, 46.5, and 48.5°C) and $\Delta\dot{P}$ (260, 320, and 380 bar/s). In these ranges the system has proved to be foamable without appreciable collapse of the cellular structure or premature crystallization [21]. By using three values for each process parameter a set of nine experiments was set, in order to obtain a complete linear 3D model: T_{foam}-parametric planes in the (final property-P_{sat}-$\Delta\dot{P}$) space, P_{sat}-parametric planes in the (final property-T_{foam}-$\Delta\dot{P}$) space and, finally, $\Delta\dot{P}$-parametric planes in the (final property-T_{foam}-P_{sat}) space. A further arbitrarily chosen experiment was used to confirm model prediction.

Four experiments were made for each test condition. The experimental values reported in Table 2, both for the densities and the cell

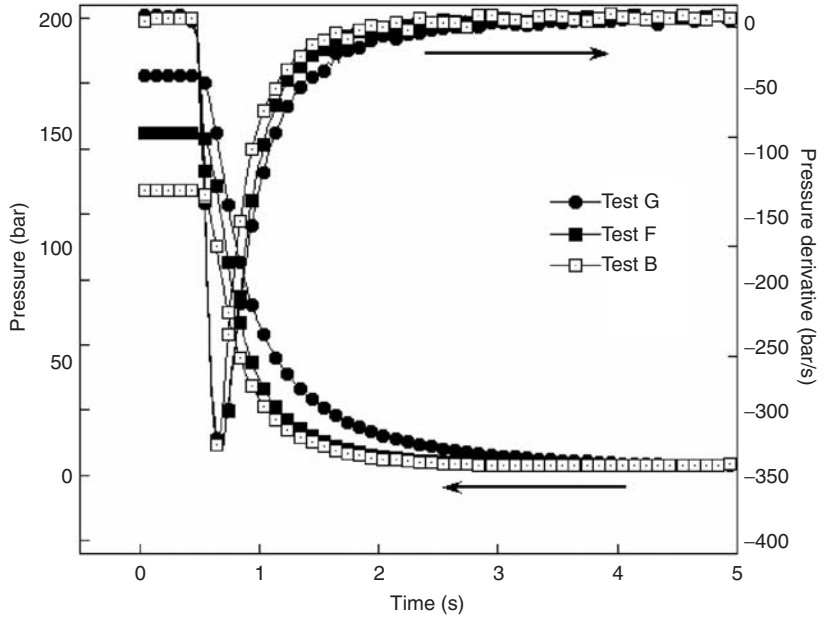

Figure 2. Pressure histories and their time derivatives for tests B ($P_{sat} = 140$ bar), F ($P_{sat} = 170$ bar), and G ($P_{sat} = 200$ bar), $\Delta\dot{P} = 320$ bar/s.

diameters, are the mean values obtained by these experiments. The standard deviation obtained from the experimental determination of the foams density was 10 kg/m^3, while for cells dimension was 35 μm.

The pressure discharge system allowed the independent control of gas saturation pressure and the rate at which gas was released from the pressure vessel. In particular, in Figure 2 the pressure histories, for tests B, F, and G and their time derivatives are reported. It is worth of note that equal pressure drop rate were obtained even if the starting pressures were different. Figure 3 reports the pressure histories, $P(t)$'s, and their derivatives for tests I, G, and H. Different pressure drop rates were obtained even if the same saturation pressure, $P_{sat} = 200$ bar, was used.

Foam Characterization

The foams were characterized to determine their densities, cell densities and mean cell diameters. The density was determined, according to ASTM D792, by weighting the sample mass in air and

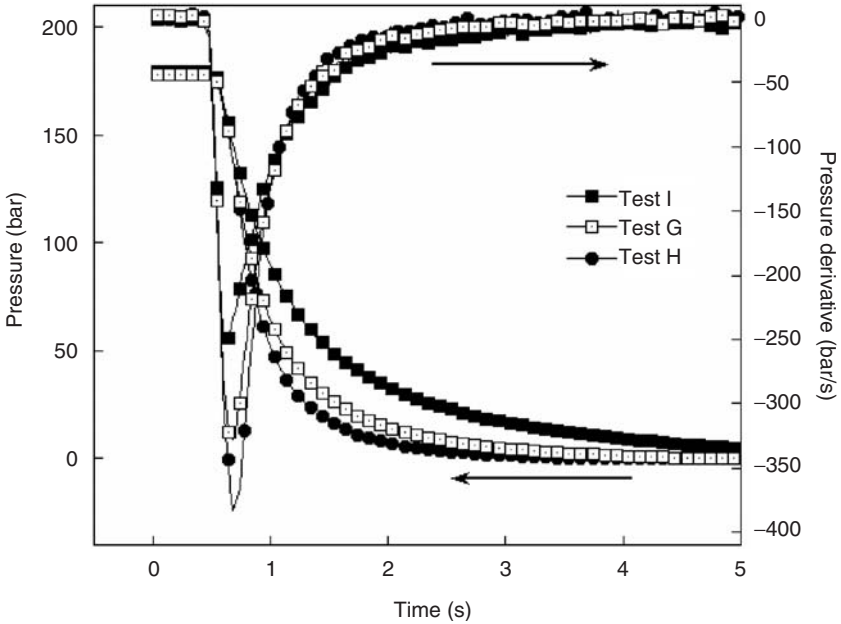

Figure 3. Pressure histories and their time derivatives for tests I ($\Delta\dot{P} = 260$ bar/s), G ($\Delta\dot{P} = 320$ bar/s), and H ($\Delta\dot{P} = 380$ bar/s), $P_{sat} = 200$ bar.

dividing this value by the volume of water displaced by the sample. The cellular structure of the foams was investigated using a LEICA S440 scanning electron microscope. The samples were first sectioned in liquid nitrogen and coated with gold using a sputter coater (Emscope SC500). The cell number density (the number of cells per cubic centimeter relative to the non-foamed polymer), and the mean cell diameter were determined from SEM micrographs as described in [3].

RESULTS AND DISCUSSION

The complete set of experiments, reported in Table 1, was chosen with the aim of investigating the correlation between process parameters and final characteristics of foams with minimal experimental effort. The determination of the planes describing the dependence between the foam properties and the process parameters needs three experimental points and, hence, three values for each parameter (for example, tests B, E, and H to obtain the plane reporting the effect of P_{sat} and $\Delta\dot{P}$ on the foam density, when the foaming temperature was 46.5°C). Moreover, this allowed a first-order (linear)

description of the effect of the processing variables on the foam structure (i.e., foam density and mean cell diameter as linear functions of the three processing variables). To do so, in order to reduce non-linearities, the investigated experimental processing window was very narrow. Both theoretical models and experimental data reported on thermoplastic foaming describe strong non-linearities and complex dependencies between process variables and final foam structures. The claimed linearity is not intended to contradict these findings but is a rough simplification, made possible by the very narrow experimental range.

The experimental results are both visualized as planes in a 3D space (in which a characteristic of the foam was plotted as function of two process parameters while holding the third at a fixed value), and described as linear algebraic functions of the three parameters.

The graphic visualization was obtained by the planes passing through the three experimental points. Each point is characterized by the test process variables and the measured experimental value of the final property (density or mean cell diameter). The analytical representation was obtained by fitting all of the experimental data with the following:

$$P = A \times (T_{\text{foam}}) + B \times (P_{\text{sat}}) + C \times (\Delta\dot{P}) + D \tag{1}$$

in which P is the structural property of the foam (foam density or mean cell diameter) and A, B, C, and D are obtained through the fitting procedure.

Density-process Variables Dependence

The experimental batch foaming results are reported in Figure 4, described as 3D plot of the final foam density as function of saturation pressure and pressure drop rate, at the three different foaming temperatures. Only three points for each temperature (for example, tests A, D, and G for $T_{\text{foam}} = 44.5^{\circ}\text{C}$) are sufficient to draw the planes and describe the combined effect of the two variables (P_{sat} and $\Delta\dot{P}$), if the experimental range is narrow enough. What one can immediately observe is that the three planes are almost parallel to each other and move upward with the decrease of temperature: in the examined experimental range, the foam density decreases with the increase of temperature. This effect can be explained by considering that bubbles grow against the viscous forces, which decrease with the increase of the temperature. In effect, as reported for different polymer/gas systems

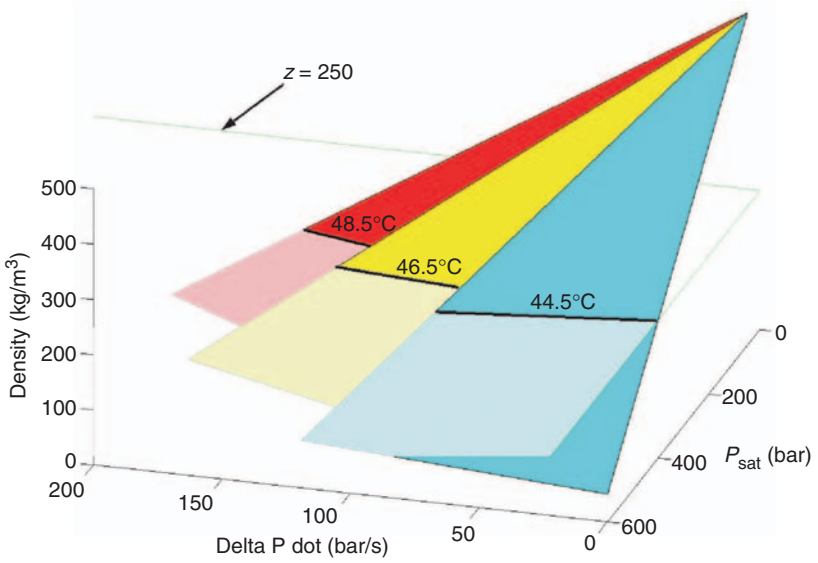

Figure 4. T_{foam}-parametric planes in the density-P_{sat}-$\Delta\dot{P}$ space.

[6,13,25,26], foam density reduces with the increase of temperature until a minimum is reached and then increases due to the bubble coalescence or collapse, leading the classical bell shape. Our experimental temperature window covers the left side of this bell shape. Therefore, if no bubble coalescence/collapse takes place, bubbles grow more easily when the temperature increases. Furthermore, a density reduction with the increase of the gas concentration, independently from the foaming temperature can be observed. This behavior is due to the blowing agent availability in the polymeric solution. The higher the saturation pressure, the higher is the weight fraction of gas in the solution and, if no collapse foams occurs, the lower are the densities. A reduced dependence of the pressure drop rate on the densities is observed, furthermore, in the investigated experimental range.

In order to facilitate this visualization, it is also possible to section the graph by iso-density planes in the density-saturation pressure-pressure drop rate 3D space. In Figure 4 is reported, as an example, the intersection of the isodensity plane (density equal to 250 kg/m^3) with the iso-temperature planes. The continuous lines describe the combination of processing parameters (i.e., saturation pressure and pressure drop rate) that will all give, at a certain temperature, foams having density of 250 kg/m^3.

A different way to represent the density-process variables dependence of the PCL/N_2 system is to fit the experimental data with a linear equation of the three variables (T_{foam}, P_{sat}, and $\Delta\dot{P}$). Fitting of experimental density data by Equation (1) yields:

$$\rho = -3.2 \times 10^{-6}(T_{foam}) - 2.5 \times 10^{-8}(P_{sat}) - 5 \times 10^{-10}(\Delta\dot{P}) + 0.35 \times 10^{-3} \quad (2)$$

in which ρ is expressed in kg/m^3, T_{foam} in °C, P_{sat} in bar and $\Delta\dot{P}$ in bar/s. In Table 2 the measured and calculated densities are reported. The standard deviation between them is 19 kg/m^3. By analyzing this equation it is possible to observe that foaming temperature has the greatest effect on foams density, with a decrease of the density when increasing temperature, as already discussed; saturation pressure increase reduces the density of foams but its influence is limited if compared with the effect of T_{foam}; finally a rather limited influence of pressure drop rate can be observed. Our equation, obviously, is not able to describe the bell shape of density versus foaming temperature reported by many authors for different polymer/gas systems [6,9,12,13,25], being just a limited part of the bell-shaped curve. In particular, as already mentioned, we analyzed a temperature range in which no coalescence/cell collapse takes place.

Morphology-process Variables Dependence

As described for foam density, a graph of the mean cell diameter as function of the process variables can be drawn to analyze their effect on the cellular morphology. In Figure 5 experimental data are described as 3D plot of the final mean cell diameters as function of saturation pressure and pressure drop rate, at the three different foaming temperatures. Differently from the density dependence on the process parameters, in this case the 3D representation is quite difficult to visualize. In order to better understand the foaming behavior of PCL/N_2 system in the examined range of process parameters, the analytical representation can be used (Equation 3). This dependence, as previously described, has been obtained by fitting all the experimental data, in terms of mean cell diameter, with a linear function of the three process variables (standard deviation is 27 μm), yielding:

$$\phi = 10 \times (T_{foam}) - 2 \times (P_{sat}) - 0.2 \times (\Delta\dot{P}) + 50 \quad (3)$$

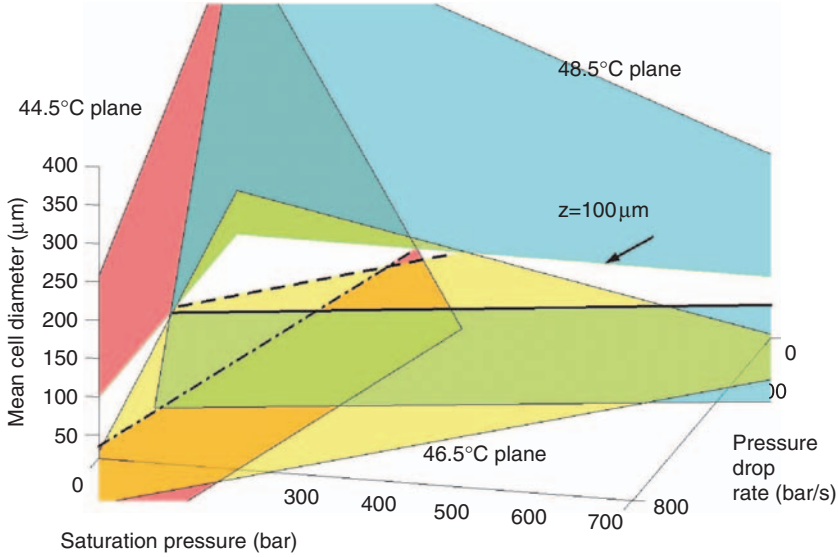

Figure 5. P_{sat}-parametric planes in the density-T_t-$\Delta\dot{P}$ space.

in which ϕ is expressed in μm. In Table 2 the cell sizes measured and calculated by using Equation 3 are reported.

By analyzing this model equation, it can be observed that mean cell diameter increases with T_{foam}. This trend, as previously described, is connected to the viscosity reduction of polymeric solution that allows greater cell walls deformation, if no cell collapse occurs. Conversely, a decrease in the cells dimension is observed when saturation pressure increases. As predicted by the classical nucleation theory, in effect, when all the other process parameters are fixed, the greater gas availability contributes to enhancing nucleation rate and, as a consequence, the final cell number. The same effect is observed when increasing pressure drop rate. In this case, however, as first discussed by Park et al. [30], cell nucleation and growth compete in consuming the available foaming agent. Pressure drop rate increase is responsible for a reduction of cell growth in favor of cell nucleation, affecting foam morphology by finally increasing the final cell number. This effect reveals a synergistic role of these two processing parameters in controlling foam morphology. Therefore, the effect of an increase of pressure drop rate on morphology is similar to the effect of an increase of saturation pressure. However, the latter is a thermodynamic effect (as predicted by classical nucleation theory [22]) while the former is a kinetic effect.

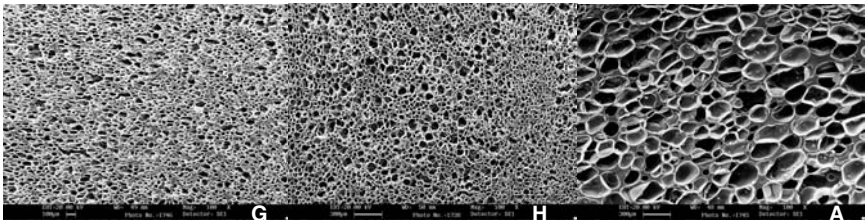

Figure 6. SEM micrographs of selected foams (see Table 1 for experimental conditions).

In Figure 5, moreover, we have sectioned the graph with an iso-diameter plane (corresponding to 100 μm). This plot shows that, in order to achieve foam structures characterized by the same mean cell diameter, the pressure drop rate should always be increased if the saturation pressure decreases. Same conclusions have been drawn by Arora et al. [9] for the two processing variables. In effect, they reported a reduction of mean cell diameter when increasing saturation pressure at constant pressure drop rate and, conversely, an increase of mean cell diameter with a reduction of pressure drop rate at a constant saturation pressure.

As a final comment on these results, it can be noted that, by optimally cross-exchanging the foaming variables it was possible to achieve foams with similar densities and different foam morphologies or similar cell morphology and very different densities (Figure 6). In particular, test G gave cellular morphology similar to H (mean cell diameter equal to 53 and 56 μm, respectively) but different densities (231 and 179 kg/m^3), while A and G showed similar densities (213 and 231 kg/m^3) but different cell morphologies (mean cell diameter equal to 161 and 53).

These examples demonstrate the capability of this approach to give foams with very controlled structures, adequate to be used, after further characterization (e.g., mechanical, insulating) for modeling the structure-properties dependences.

CONCLUSIONS

The foaming behavior of PCL/N_2 system was studied in this article. In particular, the effects of the main process parameters on the final foam characteristics were evaluated. Foaming temperature, pressure saturation and pressure drop rate were used as process variables and were varied independently to evaluate their effects on foam density

and morphology. The accurate control and the measurement of the pressure drop rate during batch foaming, and decoupling between pressure drop rate and saturation pressure, were achieved by modifying the pressure vessel through the use of capillaries with different lengths and diameters, an electronic actuated ball valve and a data acquisition system for the pressure in the vessel. Process variables' range was chosen in order to describe their effect on the foam structure by linear dependences, reported by 3D graphs or by linear equations, which resulted from fitting of the experimental results. PCL foams with tailored densities and morphologies were finally produced.

REFERENCES

1. Klempner, D. and Frisch, K.C. (1991). *Polymeric Foams*, Hanser, New York.
2. Throne, J.L. (1996). *Thermoplastic Foams*, Sherwood Publishers, Hinckley, OH.
3. Park, C.B. and Cheung, L.K. (1997). A Study of Cell Nucleation in the Extrusion of Polypropylene Foams, *Polym. Eng. Sci.*, **37**(1): 1–10.
4. Naguib, H.E., Wang, J., Park, C.B., Mukhopadhyay, A. and Reichelt, N. (2003). Effect of Recycling on the Rheological Properties and Foaming Behaviors of Branched Polypropylene, *Cell. Polym.*, **22**(1): 1–21.
5. Naguib, H.E., Park, C.B., Panzer, U. and Reichelt, N. (2002). Strategies for Achieving Ultra Low-density Polypropylene Foams, *Polym. Eng. Sci.*, **42**(7): 1481–1492.
6. Naguib, H.E., Park, C.B. and Reichelt, N. (2004). Fundamental Foaming Mechanisms Governing the Volume Expansion of Extruded Polypropylene Foams, *J. Appl. Polym. Sci.*, **91**(4): 2661–2668.
7. Nam, G.J., Yoo, J.H. and Lee, J.W. (2005). Effect of Long-Chain Branches of Polypropylene on Rheological Properties and Foam-extrusion Performances, *J. Appl. Polym. Sci.*, **96**(5): 1793–1800.
8. Park, C.B., Behravesh, H. and Venter, R.D. (1998). Low Density Microcellular Foam Processing in Extrusion Using CO_2, *Polym. Eng. Sci.*, **38**(11): 1812–1823.
9. Arora, K.A., Lesse, A.J. and McCarthy, T.J. (1998). Preparation and Characterization of Microcellular Polystyrene Foams Processed in Supercritical Carbon Dioxide, *Macromolecules,* **31**(14): 4614–4620.
10. Stafford, C.M., Russell, T.P. and McCarthy, T.J. (1999). Expansion of Polystyrene Using Supercritical Carbon Dioxide: Effects of Molecular Weight, Polydispersity, and Low Molecular Weight Components, *Macromolecules*, **32**(22): 7610–7616.
11. Xu, X., Park, C.B., Xu, D. and Pop-Iliev, R. (2003). Effects of Die Geometry on Cell Nucleation of PS Foams Blown With CO_2, *Polym. Eng. Sci.*, **43**(7): 1378–1390.
12. Liang, M.T. and Wang, C.M. (2000). Production of Engineering Plastics Foams by Supercritical CO_2, *Ind. Eng. Chem. Res.*, **39**(12): 4622–4626.

13. Lee, J.W.S., Wang, K. and Park, C.B. (2005). Challenge to Extrusion of Low-density Microcellular Polycarbonate Foams Using Supercritical Carbon Dioxide, *Ind. Eng. Chem. Res.*, **44**(1): 92–99.
14. Gendron, R. and Daigneault, L.E. (2003). Continuous Extrusion of Microcellular Polycarbonate, *Polym. Eng. Sci.*, **43**(7): 1361–1377.
15. Ray, S.S. and Okamoto, M. (2003). New Polylactide/Layered Silicate Nanocomposites, 6[a] Melt Rheology and Foam Processing, *Macromol. Mater. Eng.*, **288**(12): 936–944.
16. Fujimaoto, Y., Ray, S.S., Okamoto, M., Ogami, A., Yamada, K. and Ueda, K. (2003). Well-controlled Biodegradable Nanocomposite Foams: From Microcellular to Nanocellular, *Macromol. Rapid Commun.*, **24**(7): 457–461.
17. Di, Y., Iannace, D., Di Maio, E. and Nicolais, L. (2005). Poly(lactic acid)/ Organoclay Nanocomposites: Thermal, Rheological Properties and Foam Processing, *J. Polym. Sci., Part B: Polym. Phys.*, **43**(6): 689–698.
18. Coombes, A.G.A., Rizzi, S.C., Williamson, M., Barralet, J.E., Downes, S. and Wallace, W.A. (2004). Precipitation Casting of Polycaprolactone for Applications in Tissue Engineering and Drug Delivery, *Biomaterials*, **25**(2): 315–325.
19. Xu, Q., Ren, X., Chang, Y., Wang, J., Yu, L. and Dean, K. (2004). Generation of Microcellular Biodegradable Polycaprolactone Foams in Supercritical Carbon Dioxide, *J. Appl. Polym. Sci.*, **94**(2): 593–597.
20. Cotugno, S., Di Maio, E., Mensitieri, G., Iannace, S., Roberts, G.W., Carbonell, R.G. and Hopfenberg, H.B. (2005). Characterization of Microcellular Biodegradable Polymeric Foams Produced from Supercritical Carbon Dioxide Solutions, *Ind. Eng. Chem. Res.*, **44**(6): 1795–1803.
21. Di Maio, E., Mensitieri, G., Iannace, S., Nicolais, L., Li, W. and Flumerfelt, R.W. (2005). Structure Optimization of Polycaprolactone Foams by Using Mixtures of CO_2 and N_2 as Blowing Agents, *Polym. Eng. Sci.*, **45**(3): 432–441.
22. Goel, S.K. and Beckman, E.J. (1994). Generation of Microcellular Polymeric Foams Using Supercritical Carbon Dioxide. I: Effect of Pressure and Temperature on Nucleation, *Polym. Eng. Sci.*, **34**(14): 1137–1147.
23. Lee, K.N., Lee, H.J. and Kim, J.H. (2000). Preparation and Morphology Characterization of Microcellular Styrene-co-acrylonitrile (SAN) Foam Processed in Supercritical CO_2, *Polym. Int.*, **49**(7): 712–718.
24. Krause, B., Mettinkhoff, R. and Van der Vegt, N.F.A. (2001). Microcellular Foaming of Amorphous High-T_g Polymers using Carbon Dioxide, *Macromolecules*, **34**(4): 874–884.
25. Handa, P.Y., Wong, B. and Zhang, Z. (1999). Some Thermodynamic and Kinetic Properties of the System PETG-CO_2, and Morphological Characteristics of the CO_2-Blown PETG Foams, *Polym. Eng. Sci.*, **39**(1): 55–61.
26. Krause, B., Sijbesma, H.J.P., Münüklü, P., Van der Vegt, N.F.A. and Wessling, M. (2001). Bicontinuous Nanoporous Polymers by Carbon Dioxide Foaming, *Macromolecules*, **34**(25): 8792–8801.

27. Rezgui, F., Swistek, M., Hiver, J.M., G'Sell, C. and Sadoun, T. (2005). Deformation and Damage Upon Stretching of Degradable Polymers (PLA and PCL), *Polymer*, **46**(18): 7370–7385.
28. Kweon, H.Y., Yoo, M.K., Park, I.K. and Kim, T.H. (2003). A Novel Degradable Polycaprolactone Networks for Tissue Engineering, *Biomaterials*, **24**(5): 801–808.
29. Ray, S.S. and Bousmina, M. (2005). Biodegradable Polymers and their Layered Silicate Nanocomposite: In Greening the 21st Century Materials World, *Prog. Mater. Sci.*, **50**: 962–1079.
30. Park, C.B., Baldwin, D.F. and Suh, N.P. (1995). Effect of the Pressure Drop Rate on Cell Nucleation in Continuous Processing of Microcellular Polymers, *Polym. Eng. Sci.*, **35**(5): 432–440.